Variability in individual particle structure and mixing states between the glacier snowpack and atmosphere interface in the northeast Tibetan Plateau

Zhiwen Dong [a, b, *], Shichang Kang [a, c], Dahe Qin [a], Yaping Shao [b], Sven Ulbrich [b], Xiang Qin [a, d]

[a] State Key Laboratory of Cryosphere Sciences, Northwest Institute of Eco-Environment and Resources, Chinese Academy of Sciences, Lanzhou 730000, China;

[b] Institute for Geophysics and Meteorology, University of Cologne, Cologne D-50923, Germany;

[c] CAS Center for Excellence in Tibetan Plateau Earth Sciences, Beijing 100101, China;

[d] Qilian Shan Station of Glaciology and Ecological Environment, Chinese Academy of Sciences, Lanzhou 730000, China.

*** Corresponding Author. E-mail Address:** dongzhiwen@lzb.ac.cn (Z. Dong).

Abstract

Aerosols affect the earth's temperature and climate by altering the radiative properties of the atmosphere. Changes in the composition, morphology structure and mixing states of aerosol components will cause significant changes in radiative forcing in the atmosphere. This work focused on the physicochemical properties of light-absorbing particles (LAPs) and their variability through deposition process from the atmosphere to the glacier/snowpack interface based on large-range observation in northeast Tibetan Plateau, and laboratory transmission electron microscope (TEM) and energy dispersive X-ray spectrometer (EDX) measurements. The results showed that LAPs particle structures changed markedly in the snowpack compared to those in the atmosphere due to black carbon (BC)/organic matter (OM) particle aging and salt-coating condition changes. Considerably more aged BC and OM particles were observed in the glacier and snowpack surfaces than in the atmosphere, as the concentration of aged BC and OM

varied in all locations by 4%-16% and 12%-25% in the atmosphere, respectively, whereas they varied by 25%-36% and 36%-48%, respectively, in the glacier/snowpack surface. Similarly, the salt-coated particle ratio of LAPs in the snowpack is lower than in the atmosphere. Albedo change contribution in the Miaoergou, Yuzhufeng and Qiyi Glaciers is evaluated using the SNICAR model for glacier surface distributed impurities. Due to the salt-coating state change, the snow albedo decreased by 16.7%-33.9% compared to that in the atmosphere. Such great change may cause more strongly enhanced radiative heating than previously thought, suggesting that the warming effect from particle structure and mixing change of glacier/snowpack LAPs may have markedly affected the climate on a global scale in terms of direct forcing in the Cryosphere.

Keywords: light-absorbing aerosols; atmosphere-snowpack interface; BC/OM particle structure aging; salt-coating change; particle internal mixing

1. Introduction

Aerosols affect the earth's temperature and climate by altering the radiative properties of the atmosphere (Jacobson, 2001, 2014; Ward et al., 2018). Snow cover and glaciers in cryospheric regions play an important role in global climate change because of their large areas of distribution on the earth's surface, especially in the Northern Hemisphere, e.g., in the Alpine Mountains, the Tibetan Plateau, northern hemisphere snowpack and the Polar Regions. Individual pollutant aerosols, e.g., black carbon (BC, or soot), organic carbon (OC) or organic matter (OM), mineral dust, deposited on glacier/snowpack surfaces cause enhanced surface heat absorption, acting as light absorbing particles (LAPs), and they thus impact radiative forcing in the cryosphere. Moreover, changes in composition, morphology structure and mixing states of different LAPs components will cause significant variability in individual particle radiative heating with largely varied surface albedo due to the changes in a single particle's mixing states (Cappa et al., 2012; Peng et al., 2016).

The Tibetan Plateau, acting as the "The Third Pole" region, is one of the largest cryosphere regions with a large ice mass beside the Polar Regions (Qiu, 2008). Large amounts of LAPs particles deposited on the glacier/snowpack surface can significantly

impact surface radiative forcing, and induce increased heat absorption of the atmosphere interface in lower and middle troposphere (Anesio et al., 2009; Kaspari et al., 2011; Dong et al., 2016, 2017), thereby causing rapid glacier melting in the region (Xu et al., 2009; Zhang et al., 2017; Skiles et al., 2018; Dumont et al., 2014).

Aerosols and climate interaction has become a major concern in the Tibetan Plateau region (Dong et al., 2016, 2017). For example, the long-range transport and deposition of BC (soot), various types of salts (e.g., ammonium, nitrate and sulfate), and aerosols, and their climate significance on the Tibetan Plateau glaciers have recently become heavily researched topics (Ramanathan et al., 2007; Flanner et al., 2007; Zhang et al., 2018). However, to date, notably limited studies have focused on the composition, mixing states, and change process of LAPs particles in the atmosphere-snowpack interface of the Tibetan Plateau glacier basins. Moreover, current modeling on cryospheric snow/ice radiative forcing's impact on climate change has rarely considered such influences from changes of the single particle's structure and mixing states (Ramanathan et al., 2007; Hu et al., 2018). Because of glacier ablation and LAPs accumulation in summer, the concentration of distributed impurities in glacier/snowpack surface is often even higher than that of the atmosphere (Zhang et al., 2017; Yan et al., 2016).

Therefore, this study aimed to provide a first and unique record of the individual LAPs' physicochemical properties, components variability and mixing states between the glacier/snowpack and atmosphere interface, based on aerosol (total suspended particle (TSP) on the aerosol filter) and the glaciers/snowpack surface-distributed impurity sampling in the northeast Tibetan Plateau during June 2016 to September 2017, to determine the LAPs particle's structure aging and mixing state changes through atmospheric deposition process from the atmosphere to the glacier/snowpack surface, thereby helping to characterize the LAPs' radiative forcing and climate effects in the Cryosphere region of Tibetan Plateau. Moreover, the albedo change contributions of LAPs in several glacier surfaces (e.g. Miaoergou, Yuzhufeng and Qiyi Glaciers) were evaluated using a SNICAR (Single-layer implementation of the Snow, Ice, and Aerosol Radiation) model for the salt mixing states of surface-distributed impurities of the observed glaciers. We organized the paper as follows: In section 2, we provided detailed

descriptions about data and method of individual aerosol particle sampling and analysis; and in section 3 we presented the observed results and discussion of: (i) comparison of LAPs components between atmosphere and snowpack interface; (ii) BC/OM particle structure aging variability between atmosphere and snowpack interface; (iii) changes in salt-coating conditions and BC/OM mixing states between the atmosphere and snowpack interface; (iv) particle mixing states variability and its contribution to light absorbing. In section 4, we concluded our results and also provided the future study objective for the community.

2. Data and Methods

Field Work Observation and Sampling. The main methods of the study include the fieldwork observations, and laboratory transmission electron microscope (TEM) and energy dispersive X-ray spectrometer (EDX) instrument analysis. Atmospheric LAPs samples (TEM aerosol filter samples) and the glacier/snowpack surface distributed impurity samples were both collected across the northeastern Tibetan Plateau region in summer between June 2016 and September 2017. Figure 1 shows the sampling locations and their spatial distribution in the region, including locations in the eastern Tianshan Mountains, the Qilian Mountains, the Kunlun Mountains and the Hengduan Mountains, where large-range spatial scale observations were conducted (see Table 1). During the fieldwork sampling, we used the middle-volume-sampler (DKL-2 (Dankeli) with a flow rate of 150 L/min) for TEM filter sampling in this study, with a flow rate of 1 L min^{-1} were used for TSP filter sampling in our study, by a single-stage cascade impactor with a 0.5 mm diameter jet nozzle and an airflow rate of 1.0 L min^{-1}. Each sample was collected with 1-hour duration. After collection, the sample was placed in a sealed dry plastic tube and stored in a desiccator at 25°C and 20±3% RH to minimize exposure to ambient air before analysis, and particle smaller than 0.5 mm can be collected efficiently by the instruments. In total, 80 aerosol samples were collected directly on the calcium-coated carbon (Ca-C) grid filter. Additionally, 88 glacier/snowpack surface-snow samples were collected on the glacier/snowpack surface (with 5 cm snow depth, each sampled for 200 mL) for comparison with the deposition process, and the snow samples are taken at the same time of the atmospheric aerosol sampling. The aerosol/snow sampling method is

also the same to the previous study in Dong et al. (2016, 2017). The detailed information on sampling locations, time period and aerosol/snow sample number are shown in Table 1. Snow samples were collected at different elevations along the glacier/snowpack surfaces of the study. Pre-cleaned low-density polyethylene (LDPE) bottles (Thermo scientific), stainless steel shovel, and super-clean clothes were used for the glacier/snowpack surface-snow sample collection. All samples were kept frozen until they were transported to the lab for analysis.

TEM-EDX Microscopy Measurements. Laboratory TEM-EDX measurements were performed directly on the Ca-C filters grids (Dong et al., 2016). Ca-C grids were used as filters with the advantage of clear and unprecedented observation for single-particle analyses of aerosols and snowpack samples (Creamean et al., 2013; Li et al, 2014; Semeniuk et al., 2014). Analyses of individual particle observations were conducted using a JEM-2100F (Japan Electron Microscope) transmission electron microscope operated at 200 kV. The analyses involved conventional and high-resolution imaging using bright field mode, electron diffraction (Semeniuk, et al., 2014; Li et al., 2014), and energy-dispersive X-ray spectrometry. A qualitative survey of grids was undertaken to assess the size and compositional range of particles and to select areas for more detailed quantitative work that was representative of the entire sample. This selection ensured that despite the small percentage of particles analyzed quantitatively, our results were consistent with the qualitative survey of the larger particle population on each grid. Quantitative information on size, shape, composition, speciation, mixing state, and physical state was collected for a limited set of stable particles. Some LAPs particles, including nitrate, nitrite, and ammonium sulfate, though not stable under the electron beam, can be well detected on EDX at low beam intensity. EDX spectra were collected for 15 s in order to minimize radiation exposure and potential beam damage. All stable particles with sizes 20 nm to 35 μm were analyzed within representative grid mesh squares located near the center of the grid. Grid squares with moderate particle loadings were selected for study to preclude the possibility of overlap or aggregation of particles on the grid after sampling. The use of Ca-C grids resulted in clear and unprecedented physical and chemical information for the individual particle types. Using TEM-EDX microscope measurements, we can also easily derive the salt-coating conditions based on

the advantage of the transmission observation to obtain individual particle inside-structure (Li et al., 2014). Particle (e.g. BC, OM) with salt coating will appear clearly surrounded by various salts shell and with the BC/OM particle as the core. In general, more than 400 particles were analyzed per grid; thus, more than 1200 particles were analyzed from the three grid fractions per sample. Moreover, as the snow samples melting will affect the individual particle composition during the measurements, especially for various types of salts because the salt is unstable in high temperature (e.g. Ammonium and Nitrates) and will change, thus the snow/aerosol samples were directly observed under the TEM instrument and measured before it melted. All samples were measured in frozen states.

Snow Albedo Change Evaluation. We also simulated the albedo change contributed by individual particle mixing states' variability of LAPs. The SNICAR model can be used to simulate the albedo of snowpack by the combination of the impurity of the contents (e.g., BC, dust and volcanic ash), snow effective grain size, and incident solar flux parameters (Flanner et al., 2007). In this work, we use the online SNICAR model (http://snow.engin.umich.edu/). In the SNICAR model, the effective grain sizes of snow were derived from the stratigraphy and ranged from 100 μm for fresh clean snow to 1500 μm for aged snow and granular ice. The model was run with low, central, and high grain size for each snow type to account for the uncertainties in the observed snow grain sizes. Snow density varied with crystal size, shape, and the degree of rimming. The snow density data used in the SNICAR model are summarized with low-, central-, and high-density scenarios for the model run based on a series observations in the Tibetan Plateau and previous literature (Judson and Doesken, 2000; Sjögren et al., 2007; Zhang et al., 2018). In the model simulation, mineral dust (93.2±27.05 μg/g), BC (1517±626 μg/kg) and OC (974±197 μg/kg) average concentration data, as well as other parameters, such as effective grain size, snow density, solar zenith angle, and snow depth on the glaciers, were all considered; The mass absorption cross-sections (MAC) for salt-coated BC was referred to the average situation derived from the northern Tibetan Plateau glaciers (Zhang et al., 2017, 2018; Yan et al., 2016; Wang et al., 2013). Though showing high level, the BC concentration data used in this study is comparable to the previous work results derived from the Himalaya ice core (Ming et al., 2008), as with relatively higher

average elevation in the Everest (its deposition site elevation 6500 m a.s.l. compared to 2900-4750 m a.s.l. of northeast Tibetan Plateau glacier sampling sites) and lower atmospheric BC concentration. Besides, in this work we mainly focus on LAPs (BC, OC, mineral dust, and others) in the glaciers and snowpacks for the surface distributed impurities, thus impurity is often accumulated in summer with surface ablation and with higher BC concentration.

When running the SNICAR model, BC/OM was assumed to be coated or non-coated with sulfate (Flanner et al., 2007; Qu et al., 2014), or other salts. The mass absorption cross section (MAC) is an input parameter for the SNICAR model; it is commonly assumed to be 7.5 m^2/g at 550 nm for uncoated BC particles (Bond et al., 2013). For salt-coated BC particles, the MAC scaling factor was set to be 1 m^2/g, following Qu et al. (2014) and Wang et al. (2015). Other impurities (such as volcanic ash) were set to zero. In terms of the albedo calculation, the BC and dust radiative forcing (RF) can be obtained by using equation (1) (Kaspari et al., 2014; Yang et al., 2015):

$$\mathrm{RF} = \sum_{0.325\,\mu\mathrm{m}}^{2.505\,\mu\mathrm{m}} E(\lambda,\theta)(\alpha_{(r,\lambda)} - \alpha_{(r,\lambda,\mathrm{imp})})\Delta\lambda \quad (1)$$

where α is the modeled snow albedo with or without the impurities (imp) of BC and/or dust; E is the spectral irradiance (W m^{-2}); r is the snow optical grain size (μm); λ is wavelength (μm); and θ is the solar zenith angle for irradiance (°).

3. Results and Discussion

3.1 Comparison of LAPs Components between Atmosphere and Snowpack Interface

Figure 2 shows the component types of the individual LAPs particle found in the atmosphere and glacier/snowpack of northeast Tibetan Plateau. Based on the above microscope observations, aerosols were classified into seven components: NaCl salt, mineral dust, BC (soot)/ fly ash, sulfates, ammonium, nitrates, and organic matter (OM). Classification criteria of sampled particle types, mixing states and their possible sources

in the snow/atmosphere samples were indicated in Table S1. Figure 3 shows the comparison of individual LAPs particle components types between glacier/snowpack and atmosphere interface in northeast Tibetan Plateau region, which indicates the LAPs composition in atmosphere of various locations as BC (mean percentage of 18.3%, standard deviation (SD) 2.58), OC (28.2%, SD 3.49), NaCl (11%, SD 2.58), Sulfate (17%, SD 3.49); Ammonium (4.8%, SD 3.01), Nitrate (7%, SD 2.83), Mineral dust (13.7%, SD 3.02), whereas the LAPs composition in glacier/snowpack surface as: BC (mean 21.3%, SD 2.49), OC (31.2%, SD 2.44), NaCl (16.2%, SD 3.12), Sulfate (6.8%, SD 1.32), Ammonium (2%, SD 0.81), Nitrate (3.3%, SD 0.95), Mineral dust (19.2%, SD 2.9). We found that the impurity components show large differences between the snowpack and atmosphere in all locations, implying significant change through the aerosols' deposition processing in the interface (Figure 3). LAPs components have a large change of proportion in the interface, probably due to different atmospheric cleaning rates and atmospheric processing with dry/wet aerosol deposition. Sulfates and other salts in the atmosphere act as salt-coating forms to other particles with aggregated states and will be dissolved and taken away with precipitating snow and meltwater in the snowpack, which will cause reduced salt components (e.g., sulfate, nitrate, NaCl, and ammonium) in the glacier/snowpack surface compared to those in the atmosphere. Therefore, we can observe obvious changes in composition and mixing states of the impurities between the atmosphere and glacier/snowpack surface in Figure 3, as the ratio of BC, organic matter, and mineral dust components in the snowpack increased greatly during this process, whereas the ratio of various salts in the snowpack decreased significantly (Figure 3). The change in morphology and structure will undoubtedly cause a significant variability of impurities' heat absorbing property in both the atmosphere and the glacier/snowpack surface, and such impacts will be discussed in a later section. Moreover, the deposition flux and processing of various types of aerosol particles are different, causing the changes in composition and mixing states of LAPs impurities between the atmosphere and Cryosphere. Aerosol LAPs change during the atmospheric transport and deposition processes (especially through wet deposition with precipitating-snow) will mainly lead to large variability of individual particle's structure and morphology; for example, the particle's aging, salt-coating, and mixing states changes of BC and organic matter (with

internal or external mixing), as indicated in following sections, which will cause further influences on radiative forcing of the glacier/snowpack surface as discussed in section 3.4.

3.2 BC/OM Particle Aging between Atmosphere and Snowpack Interface

Figure 4 shows how the particle's structure changes during the individual particle aging process when deposited from the atmosphere onto the glacier snowpack surface. Figure 4a-4d is the representative particles of fresh BC/OM with fractal morphology and a large amount in the atmosphere, whereas Figure 4e-4h is the representative particles of aged BC/OM with aggregated spherical morphology in the glacier/snowpack surface. It is clear that abundant aerosol particles were observed with relatively fresh structure in the atmosphere, similar to previous studies (e.g., Li et al., 2015; Peng et al., 2016). As shown in Figure 4a-4d, the fresh aerosol particles of BC and OC (or organic matter, OM) appeared very common in the atmosphere as the main parts, whereas as shown in Figure 4e-4h, more aged particles were found deposited in the glacier/snowpack surface. This process is characterized by the initial transformation from a fractal structure to spherical morphology and the subsequent growth of fully compact particles. Previous work has indicated the structure and mass absorption cross (MAC) section change of BC particles in the atmosphere (Peng et al., 2016; Yan et al., 2016), but did not discuss such change phenomena of OM particles' change during the structure-aging process. This study reveals clearly the structure and morphology change of BC and OM particles' structure aging through the transport and deposition process to the glacier snowpack from the atmosphere (Figure 4).

Based on TEM-EDX observations, we evaluated the aged BC/OM particle composition ratio (%) in the snowpack and the atmosphere, respectively. Figure 5 shows the aging of BC/OM individual particles and their composition ratio (%) change with the deposition process from the atmosphere to the glacier/snowpack surface. Figure 5 indicates that in atmosphere the composition ratio is as fresh BC (mean percentage of 29.7%, with SD 3.95), fresh OC (41.8%, 4.34), aged BC (9.8%, 4.02), and aged OC (18.7%, 4.11); while in the snow the composition ratio is as fresh BC (mean percentage of 8.4%, SD 2.71), fresh OC (17.7%, 4.42), aged BC (31.5%, 2.99), and aged OC (42.4%, 4.45). The

proportion of aged BC and OM particles varied from 4%-16% and 12%-25% in the atmosphere, respectively, and varied from 25%-36% and 36%-48% in the glacier/snowpack surface, respectively. The amount of aged particles in snowpack is 2-3 times higher than that in the atmosphere. In the atmosphere, the BC/OM both showed high ratios of fresh structure particles (fractal morphology), while in the glacier/snowpack surface more particles indicated aged structure (spherical morphology), although there was a small portion of particles still fresh (Figure 5). The change proportion of BC/OM particle aging is very marked between the snow and the atmosphere. The particle structure is a very important factor influencing light absorbing (Peng et al., 2016); thus, such changes in BC/OM particles' structure aging between the glacier snowpack and atmosphere will actually influence the total heat absorbing of the mountain glacier/snowpack, even affecting that of the whole cryosphere on earth's surface.

3.3 Changes in Salt-Coating Conditions and BC/OM Mixing States

In addition to particle structure aging, we find evident variability in particle salt-coating conditions between the atmosphere and glacier/snowpack interface during the observation period (Figure 6). Figure 6 demonstrates the different salt-coating examples for individual aerosol particles (including BC, OM, and mineral dust) in the atmosphere in various glacier basins in the northeast Tibetan Plateau. We found that the salt-coating form is very common for impurity particles in the atmosphere, which will, of course, cause a significant influence on radiative forcing of the atmosphere. A large part of fresh BC/OM (with fractal morphology) and mineral dust particles were coated by various salts, such as sulfate, nitrates, and ammonium. Such obvious salt-coating conditions will cause reduced atmospheric radiative forcing, due to the increase of albedo (IPCC, 2013).

Similarly, we also evaluated the salt-coated particle ratio for BC/OM and its change between glacier/snowpack and atmosphere (Figure 7). Figure 7 shows the salt-coating proportion of impurity particles and its difference between the glacier/snowpack and atmosphere interface at those locations. In Figure 7, the salt-coated particles in atmosphere accounted for mean ratio of 54.61% (with SD 12.02) in various locations, while that in the snow of the glacier/snowpack was 18.59% (with SD 7.04). The

proportion of salt-coating particles varied largely from the atmosphere to the glacier/snowpack surface (2-4 times more in the atmosphere than that in snow). The change proportion of salt-coating particles is very marked, and this change will cause very complicated changes in a particle's mixing states and structure.

Figure 8 shows the situation of internal mixing states of BC (soot), organic matter (OM) and mineral dust particles in various glacier snowpacks in the region, which demonstrates the influence of the transport and deposition process to a particle's structure change. Most salts in the salt-coated particles will disappear when deposited into the glacier/snowpack surface, and the mixing states change largely to the internal and external mixing forms with BC/OM as the core. The proportion change of an internally mixed BC particle with other particles is presented in Figure 9, showing great increases in internal mixing after deposition among the locations in the whole northeast Tibetan Plateau region. As shown in Figure 9, the internally mixed particles of BC in atmosphere accounted for mean ratio 4.68% (with SD 3.07) in various locations, whereas that in the snow of glacier/snowpack was 14.85% (with SD 4.93). We find that with the salt-dissolution, a large part of LAPs particles changed to the internally mixed BC/OM particle with other aerosol particles. As a large number of particles lose the salt coating in the snowpack compared with those in the atmosphere, the whole process will certainly increase the heating absorption proportion of the LAPs. Moreover, as shown in Figure 10, average conditions of single, internally and externally mixed BC/OM individual particles in the glacier/snowpack of the northeast Tibetan Plateau changed greatly with the diameter of the particle. In Figure 10, the mixings states of BC/OC in the glacier/snowpack snow of northeast Tibetan Plateau showed that the internally, single and externally mixed BC/OC particles accounted for mean ratio of 69.2% (SD 22.5), 5.35% (SD 1.72), and 25.95% (with SD 22.4), respectively. With the increase in particle size, most BC/OM particles (PM>1 μm) showed internal mixing conditions, which will influence the RF of the glacier snowpack.

3.4 Particle Mixing States Variability and Its Contribution to Light Absorbing

Additionally, the extent of influence of LAPs' particle mixing state changes are also important and need to be evaluated for radiative forcing. The SNICAR model is often employed to simulate the hemispheric albedo of glacier/snowpack for a unique

combination of LAPs contents (e.g., BC, dust, and volcanic ash), snow effective grain size, and incident solar flux characteristics (Flanner et al., 2007). We also evaluated the influence on albedo change caused by individual particle structure and mixing state changes in the glaciers/snowpack of the northeast Tibetan Plateau region. Figure 11 showed the evaluation of snow albedo change of BC-salt coating change in the snowpack compared with that in the atmosphere using SNICAR model simulation in the MG, YG, QG, showing the albedo change of snow surface impurities in snowpack compared to that of the atmosphere. The parameters input for SNICAR model have been described in the method section. Mineral dust, BC and OC average concentration data, as well as other parameters, such as effective grain size, snow density, solar zenith angle, and snow depth on the glaciers, and MAC for BC were referred from the average situation in previous work of northern Tibetan Plateau glaciers (Zhang et al., 2017, 2018; Yan et al., 2016; Wang et al., 2013). As shown in Figure 12, the surface albedo in MG, YG, and QG decreased by 16.7%-33.9% caused by salt-coating changes, when compared to that of the hypothetical similar situation of impurities' composition as that in the atmosphere. Based on the LAPs salt-coating-induced albedo changes, RF was calculated by equation (1) for the different scenarios. The results show that the RF change caused by salt coating changes, varied between 1.6–26.3 W m^2 depending on the different scenarios (low, central, and high snow density), respectively.

Figure 12 shows a schematic diagram model for the explanation of the particle structure aging and salt-coating changes, and its total influence to the radiative forcing between the atmosphere and glacier/snowpack interface on the northeast Tibetan Plateau. From the above discussion, we find a clear variability in LAPs particles' mixing forms between the glacier/snowpack surface and atmosphere, mainly originating from the morphology changes of the LAPs particle's structure (e.g. aging of BC/OM), and salt-coating changes from increased internal mixing of BC/OC particles, as many particles without salt-coating will change to internal mixing with BC/OM particles as a core, or external mixing with BC/OM, which will also significantly influence the total RF of the mountain glaciers/snowpack in the Cryosphere as indicated in previous work (Jacobson et al., 2001). Moreover, due to glacier ablation and accumulation of various types of impurities, the concentration of impurities in the snowpack surface is often even higher than that of

the atmosphere (Zhang et al., 2017; Yan et al., 2016).

In general, as shown in Figure 12, (ⅰ) more fresh BC/OM particles were observed in the atmosphere, whereas more aged BC/OM particles were found on the glacier/snowpack surface. Aged BC/OM particles often mean stronger radiative forcing in the snowpack than in the atmosphere (Peng et al., 2015). (ⅱ) More salt-coated particles were found in the atmosphere of the glacier basin, whereas reduced salt coating was found in the glacier/snow surface. With thick salt coating, the LAPs' light- absorbing properties may not be that much stronger than the particles without coating, as most salts (sulfate, nitrates, ammonium, and NaCl) did not have strong forcing because of their weak light-absorbing property and high hygroscopicity in the mixing states (IPCC, 2013; Li et al., 2014), especially for sulfate/nitrate aggregated particles. (ⅲ) With the salt-coating decrease, more internally mixed particles of BC/OM surrounded by a well-mixed salt-shell were observed from the individual particles of LAPs in the snow-ice of the cryospheric glacier basin when compared to that of the atmosphere. Internally mixed particles of BC/OM have shown the strongest light absorption in previous modeling studies (Cappa et al., 2012; Jacobson et al., 2000), as BC acts as a cell-core particle with organic matter particles (also sometimes including some salts) surrounded. In previous study the mixing state was found to affect the BC global direct forcing by a factor of 2.9 (0.27 Wm^{-2} for an external mixture, +0.54 Wm^{-2} for BC as a coated core, and +0.78 Wm^{-2} for BC as well mixed internally) (Jacobson, 2000), and that the mixing state and direct forcing of the black-carbon component approach those of an internal mixture, largely due to coagulation and growth of aerosol particles (Jacobson et al., 2001), and also found radiative absorption enhancements due to the mixing state of BC as indicated in Cappa et al. (2012), and He et al.(2015). (ⅳ) In addition to the light-absorbing from the above particle structure change, the absorbing property of some components in the atmosphere and cryosphere (snow and ice) also show a large variability, as most mineral and OM (or OC) particles show negative radiative forcing in the atmosphere while showing positive forcing in the glacier/snowpack surface, as indicated from IPCC AR5 (2013), Yan et al. (2016), Zhang et al. (2018), and Hu et al. (2018). Thus, the light-absorbing of LAPs as a whole will increase greatly in glacier/snowpack surface environments.

Therefore, the great change of glacier/snowpack surface albedo may cause more strongly enhanced radiative heating than previously thought, suggesting that the warming effect from particle structure and mixing change of glacier/snowpack LAPs may have markedly affected the climate on a global scale in terms of direct forcing in the Cryosphere.

4. Conclusions

The results showed that the LAPs particle structure changed greatly in snowpack compared to that in the atmosphere, mainly due to particle aging (mainly BC and organic matter), and the salt coating reduction process through the impurity particle's atmospheric deposition. Much more aging BC and OM and more internally mixed BC particles were observed in glacier snowpack than in the atmosphere during the simultaneous observations; for example, the proportion of aged BC and OM varies from 4-16 % and 12-25% in the atmosphere respectively, and varies from 25-36% and 36-48% respectively in the snowpack of the cryosphere. In addition to the heat absorbing from the above LAPs particle structure change, the absorbing property of dust and OC in atmosphere and cryosphere (snow and ice) also shows a large difference.

A schematic diagram model shown in the figure linking the explanation the LAPs' structure aging and salt-coating change and comparing their influences to the radiative forcing between the atmosphere and glacier snowpack was presented in the study. The LAPs in glacier/snowpack will change to more aged and internally mixed states compared to that of the atmosphere. Thus, the light absorption of the LAPs as a whole will increase greatly in glacier snowpack environments. Moreover, we also evaluated the increase in radiative forcing caused by LAPs particle structures and mixing state changes. The albedo changes in MG, YG and QG were evaluated using the SNICAR model simulation for distributed surface impurities in the observed glaciers caused by salt coating changes, which decreased by 16.7%-33.9% compared to glacier surface with similar conditions as in the atmosphere. The RF change caused by salt coating changes, varied between 1.6–26.3 W m^2 depending on the different scenarios (low, central, and high snow density), respectively. We find that the LAPs-individual-particle related albedo and radiative forcing change in this work is of importance in understanding the contribution of individual particle structure and mixing change in atmosphere-snowpack

interface, which may have markedly affected the climate on a global scale in terms of direct forcing in the Cryosphere, and need to be further studied in future.

Acknowledgements

This work was funded by the National Natural Science Foundation of China (41671062, 41721091), the State Key Laboratory of Cryosphere Sciences (SKLCS-ZZ-2018), and the Youth Innovation Promotion Association, CAS (2015347). We also thank the field work team (especially to Li G., Li Y. and Chen S F.) in the northeast Tibetan Plateau for their logistical work and sample collections. All the data used are contained within the paper and tables, figures, and references.

References

Anesio, A.M., Hodson, A.J., Fritz, A., Psenner, R., and Sattler, B.: High microbial activity on glaciers: importance to the global carbon cycle, Global Change Biol., 15, 955-960, doi: 10.1111/j.1365-2486.2008.01758.x, 2009.

China, S., Mazzoleni, C., Gorkowski, K., Aiken, A. C., and Dubey, M. K.: Morphology and mixing state of individual freshly emitted wildfire carbonaceous particles, Nat. Commun., 4, 2122, doi: 10.1038/ncomms3122, 2013.

China, S., Scarnato, B., Owen, R. C., Zhang, B., Ampadu, M. T.: Morphology and mixing state of aged soot particles at a remote marine free troposphere site: Implications for optical properties, Geophys. Res. Lett., 42, 1243-1250, doi:10.1002/2014gl062404, 2015.

Cappa, C.D., Onasch, T.B., Massoli, P., et al.: Radiative absorption enhancements due to the mixing state of atmospheric black carbon, Science, 337, 1078-1081, doi:10.1126/science.1223447, 2012.

Creamean, J.M., Suski, K.J., Rosenfeld, D., et al.: Dust and Biological Aerosols from the Sahara and Asia Influence Precipitation in the Western U.S., Science, 339, 1572-1578, doi: 10.1126/science.1227279, 2013.

Dong, Z., Kang, S., Guo, J., Zhang, Q., Wang, X., and Qin, D.: Composition and mixing states of brown haze particle over the Himalayas along two transboundary south-north

442 transects, Atmospheric Environment, 156, 24-35, doi:10.1016/j.atmosenv.2017.02.029,
443 2017.

444 Dong, Z., Qin, D., Kang, S., Liu, Y., Li, Y., Huang, J., and Qin, X.: Individual particles of
445 cryoconite deposited on the mountain glaciers of the Tibetan Plateau: Insights into
446 chemical composition and sources, Atmos. Environ., 138, 114-124, doi:
447 10.1016/j.atmosenv.2016.05.020, 2016.

448 Dumont, M., Brun, E., Picard, G., Michou, M., Libois, Q., Petit, J.R., Geyer, M., Morin,
449 S., and Josse B.: Contribution of light-absorbing impurities in snow to Greenland's
450 darkening since 2009, Nature Geoscience, 7, 509–512, doi:10.1038/ngeo2180, 2014.

451 Flanner, M. G., Zender, C. S., Randerson, J. T., and Rasch, P. J.: Present-day climate
452 forcing and response from black carbon in snow, J. Geophys. Res. Atmos., 112, D11202,
453 2007.

454 He, C., Liou, K.N. Takano, Y. et al.: Variation of the radiative properties during black
455 carbon aging: theoretical and experimental intercomparison, Atmos. Chem. Phys., 15,
456 11967-11980, 2015.

457 He, C., Li, Q., Liou, K., Takano, Y., Gu, Y., Qi, L., Mao, Y, and Leung, L. R.: Black
458 carbon radiative forcing over the Tibetan Plateau, Geophys. Res. Lett., 41, 7806-7813,
459 doi: 10.1002/2014gl062191, 2014.

460 Hu, Z., Kang, S., Yan, F., Zhang, Y., Li, Y., Chen, P., Wang, K., Gao, S., and Li, C.:
461 Dissolved organic carbon fractionation accelerates glacier-melting: A case study in the
462 northern Tibetan Plateau, Science of the Total Environment, 627, 579-585, 2018.

463 Li, W., Chen S., Xu Y., Guo, X., Sun, Y.: Mixing state and sources of submicron regional
464 background aerosols in the northern Qinghai–Tibet Plateau and the influence of biomass
465 burning, Atmos. Chem. Phys., 15, 13365-13376, 2015.

466 Li, W., Shao, L., Shi, Z., Chen, J., Yang, L., Yuan, Q., and Yan, C.: Mixing state and
467 hygroscopicity of dust and haze particles before leaving Asian continent, J. Geophys.
468 Res., 119, 1044–1059, 2014.

469 Jacobson, M. Z.: Strong radiative heating due to the mixing state of black carbon in

atmospheric aerosols, Nature, 409, 695-697, doi: 10.1038/35055518, 2001.

Jacobson, M. Z.: A physically-based treatment of elemental carbon optics: Implications for global direct forcing of aerosols, Geophys. Res. Lett., 27, 217-220, 2000.

Kaspari, S.D., Schwikowski, M., Gysel, M., Flanner, M. G., Kang, S., Hou, S., Mayewski, P. A.: Recent increase in black carbon concentrations from a Mt. Everest ice core spanning 1860-2000 AD, Geophys. Res. Lett., 38, L04703, 2011.

Martins, J. V., Artaxo, P., Liousse, C., Reid, J. S., Hobbs, P. V., and Kaufman, Y. J.: Effects of black carbon content, particle size, and mixing on light absorption by aerosols from biomass burning in Brazil, J. Geophys. Res. Atmos., 103, 32041–32050, doi: 10.1029/98jd02593, 1998.

Ming J., Cachier H., Xiao C., Qin, D., Kang, S., Hou, S., and Xu, J.: Black carbon record based on a shallow Himalayan ice core and its climatic implications, Atmos. Chem. Phys., 8, 1343–1352, 2008.

Peng, J., Hu, M., Guo, S., Du, Z., Zheng, J., et al.: Markedly enhanced absorption and direct radiative forcing of black carbon under polluted urban environments, PNAS, www.pnas.org/cgi/doi/10.1073/pnas.1602310113, 2016.

Qiu, J.: The third pole, Nature, 454, 393-396, http://dx.doi.org/10.1038/454393a, 2008.

Ramanathan, V., Ramana, M., Roberts, G., Kim, D., Corrigan, C., Chung, C., and Winker, D.: Warming trends in Asia amplified by brown cloud solar absorption, Nature, 448, 575-578, 2007.

Skiles, S. M., Flanner, M., Cook, J. M., Dumont, M., and Painter, T.H.: Radiative forcing by light-absorbing particles in snow, Nature Climate Change, doi: https://doi.org/10.1038/s41558-018-0296-5, 2018.

Semeniuk, T.A., Bruintjes, R.T., Salazar, V., Breed, D.W., Jensen, T.L., and Buseck, P.R.: Individual aerosol particles in ambient and updraft conditions below convective cloud bases in the Oman mountain region, J. Geophys. Res. Atmos., 119, http://dx.doi.org/10.1002/2013JD021165, 2014.

Wang, X., Doherty, S., and Huang, J.: Black carbon and other light-absorbing impurities in snow across Northern China, J. Geophys. Res. Atmos., 118, 1471-1492, https://doi.org/10.1029/2012JD018291, 2013.

Ward, J. L., Flanner, M. G., Bergin, M., Dibb, J. E., Polashenski, C. M., Soja, A. J., and Thomas, J. L.: Modeled response of Greenland snowmelt to the presence of biomass burning-based absorbing aerosols in the atmosphere and snow, Journal of Geophysical Research: Atmospheres, 123, https://doi.org/10.1029/2017JD027878, 2018.

Xu, B., Cao, J., Hansen, J., Yao, T.: Black soot and the survival of Tibetan glaciers, Proc. Natl. Acad. Sci. U.S.A., 106(52), 22,114–22,118, doi:10.1073/pnas.0910444106, 2009.

Yan, F., Kang, S., Li, C., Zhang, Y., Qin, X., Li, Y., Zhang, X.: Concentration, sources and light absorption characteristics of dissolved organic carbon on a medium-sized valley glacier, northern Tibetan Plateau, The Cryosphere, 10, 2611-2621, 2016.

Zhang, Y., Kang, S., Sprenger, M., Cong, Z., Gao, T., Li, C., and Tao, S.: Black carbon and mineral dust in snow cover on the Tibetan Plateau, The Cryosphere, 12, 413–431, 2018.

Zhang, Y., Kang, S., Cong, Z., Schmale, J., Sprenger, M., Li, C., Yang, W., Gao, T., Sillanpää, M., Li, X., Liu, Y., Chen, P., Zhang, X.: Light-absorbing impurities enhance glacier albedo reduction in the southeastern Tibetan plateau, J. Geophys. Res. Atmos., 122, doi: 10.1002/2016JD026397, 2017.

Tables

Table 1. Sampling locations, sampling dates, and cryoconite-snow depth at mountain glaciers of the northeast Tibetan Plateau

Sites	Glacier	Mountains	Locations	Altitude (m a.s.l.)	Sampling Date	Number Snow/Aerosols	Particles Calculated
MG	Miaoergou Glacier	Tianshan Mountains	42.59°N, 94.16°E	3800-4200	12-13 June 2017	8/8	>1200
LG12	Laohugou Glacier No.12	Qilian Mountains	39.20°N, 96.34°E	4300-4700	10-25 July, 2016, 3-8 June, 10-21 August 2017	20/24	>1200
QG	Qiyi Glacier	Qilian Mountains	39.14°N, 97.45°E	4200-4750	10-12 June 2017 20-22 August 2017	11/8	>1200
DS	Daban Snowpack	Daban Mountains	37.21°N, 101.24°E	3500-3700	3-4 June 2017	8/4	>1200
LG	Lenglongling Glacier	Qilian Mountains	37.51°N, 101.54°E	3558-3990	5-7 June 2017	12/5	>1200
SG	Shiyi Glacier	Qilian Mountains	38.21°N, 99.88° E	3900-4400	3-4 June 2017	9/6	>1200
YG	Yuzhufeng Glacier	Kunlun Mountains	35.41°N, 94.16°E	4300-4720	12 June 2017	12/11	>1200
GS	Gannan Snowpack	Gannan Plateau	34.2°N, 103.5°E	2900-3200	4-8 May 2017 6-9 August 2017	6/6	>1200
DG	Dagu Glacier	Hengduan Mountains	33°N, 101°E	3200-3900	20-22 Sept 2017	2/3	>1200
HG	Hailuogou Glacier	Hengduan Mountains	31°N,101°E	2900-3500	11-12 August 2017	6/4	>1200

Figure Captions

Figure 1 Location map showing the sampled glaciers and snowpack in the northeast Tibetan Plateau, including the Miaoergou Glacier (MG), Laohugou Glacier No.12 (LG12), Qiyi Glacier (QG), Lenglongling Glacier (LG), Shiyi Glacier (SG), Dabanshan snowpack (DS), Yuzhufeng Glacier (YG), Gannan Snowpack (GS), Dagu Glacier (DG), and Hailuogou Glacier (HG), where large-range field observations of atmosphere and glacier surface impurities were conducted.

Figure 2 Component types of individual haze particles in northwest China. Based on the above microscope observation, aerosols were classified into seven type components: NaCl salt, mineral dust, fly ash, BC (soot), sulfates, nitrates, and organic matter.

Figure 3 Comparison of individual particles' compositions of light-absorbing impurities in the (a) atmosphere and (b) glacier/snowpack surface in the northeast Tibetan Plateau, and (c) a photo of snowpack and glaciers in the Qilian Mountains taken from flight in autumn 2017, showing large distribution of snow cover and glaciers in the north Tibetan Plateau region -round.

Figure 4 Structure change during the aging of individual black carbon (BC) / organic matter (OM) particles when deposited from the atmosphere onto snow and ice surface. Figures 4a-4d is representative of atmosphere, while Figure 4e-4h shows the condition of glacier/snowpack.

Figure 5 LAPs aging of BC/OC individual impurity particles and composition ratio (%) change during the deposition process from the atmosphere to glacier snowpack, in the figure (a) is the atmosphere, and (b) is the snowpack.

Figure 6 Examples of different salt-coating conditions of BC, OM and dust for individual particles in the atmosphere of various glacier basins in northeast Tibetan Plateau

Figure 7 Salt-coating proportion changes of individual impurity particles between glacier snowpack and atmosphere in various locations of northeast Tibetan Plateau

Figure 8 Internal mixing states of BC (soot) and OM in the various glacier snowpack in

northeast Tibetan Plateau in summer 2016-2017

Figure 9 The proportion change of internally mixed BC particle with other particles，showing the obvious increase of internally mixed BC/OM in glacier snowpack compared with those in the atmosphere in summer 2016-2017

Figure 10 Average conditions of single, internally and externally mixed BC/OM individual particles in the snowpack of northeast Tibetan Plateau glaciers, showing most of the BC/OM with diameter >1 μm in internally mixing conditions.

Figure 11 Evaluation of snow albedo change of BC-salt coating change in the snowpack compared with atmosphere using SNICAR model simulation in the MG (a, b), YG (c, d), LG 12 (e, f), which shows the largely decreased albedo of snow surface impurities in snowpack compared to that of the atmosphere, implying markedly enhanced radiative forcing in the snowpack surface impurities.

Figure 12 Schematic diagram linking aging and salt coating change and comparing its influence to the radiative forcing between the atmosphere and snowpack of a remote glacier basin, thereby causing markedly enhanced heat absorption.

582

583

584

585 **Figure 1**

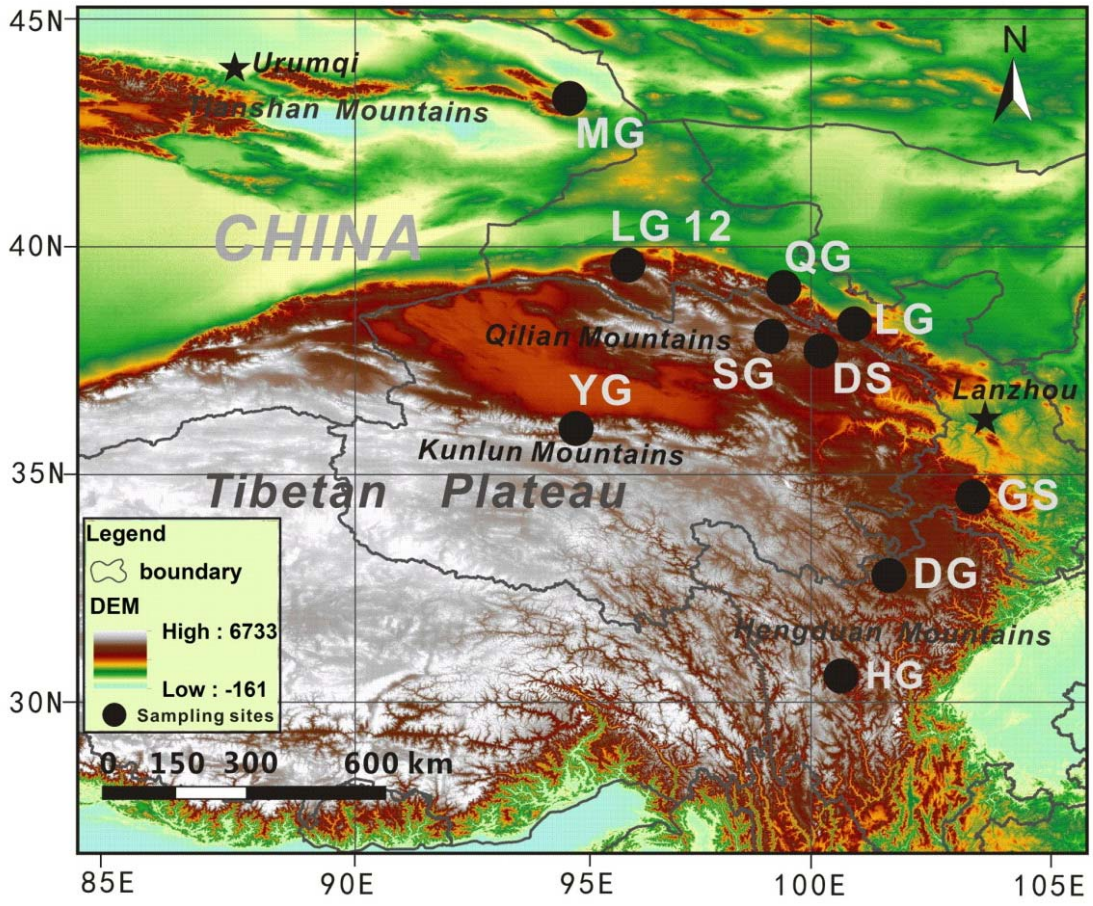

586

587

588

589

590

591

Figure 2

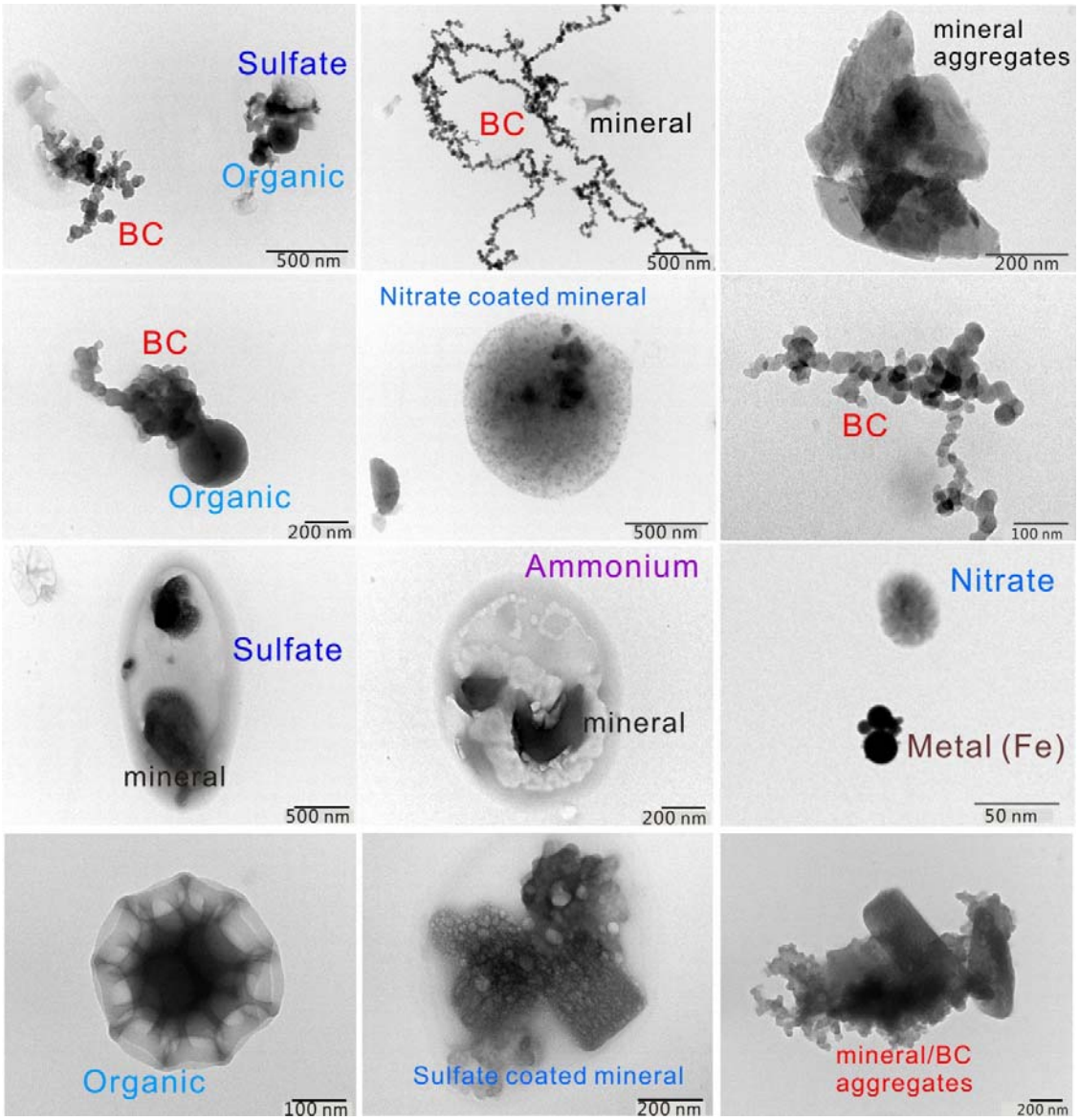
Sulfate
Organic
BC
500 nm
BC
mineral
500 nm
mineral
aggregates
200 nm
BC
Organic
200 nm
Nitrate coated mineral
500 nm
BC
100 nm
Sulfate
mineral
500 nm
Ammonium
mineral
200 nm
Nitrate
Metal (Fe)
50 nm
Organic
100 nm
Sulfate coated mineral
200 nm
mineral/BC
aggregates
200 nm

600

601

602

603 **Figure 3**

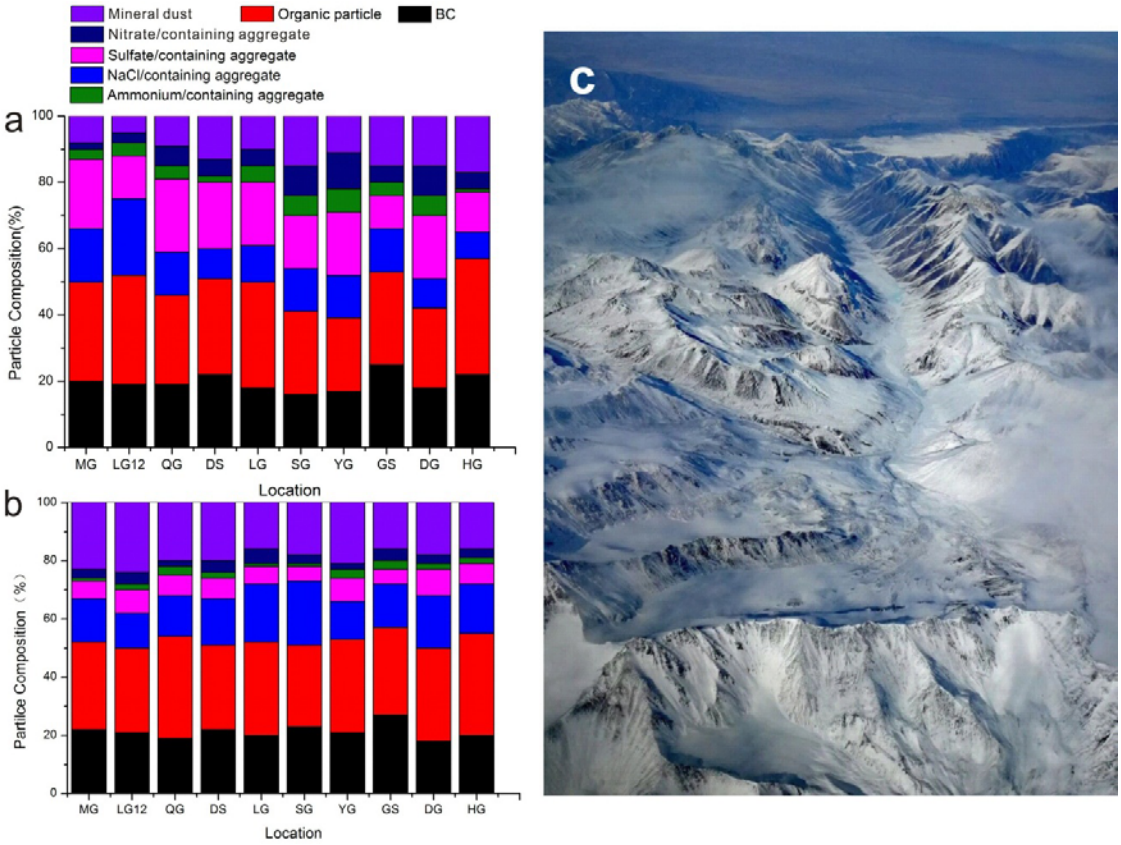

604

605

606

607

608

609

610

611 **Figure 4**

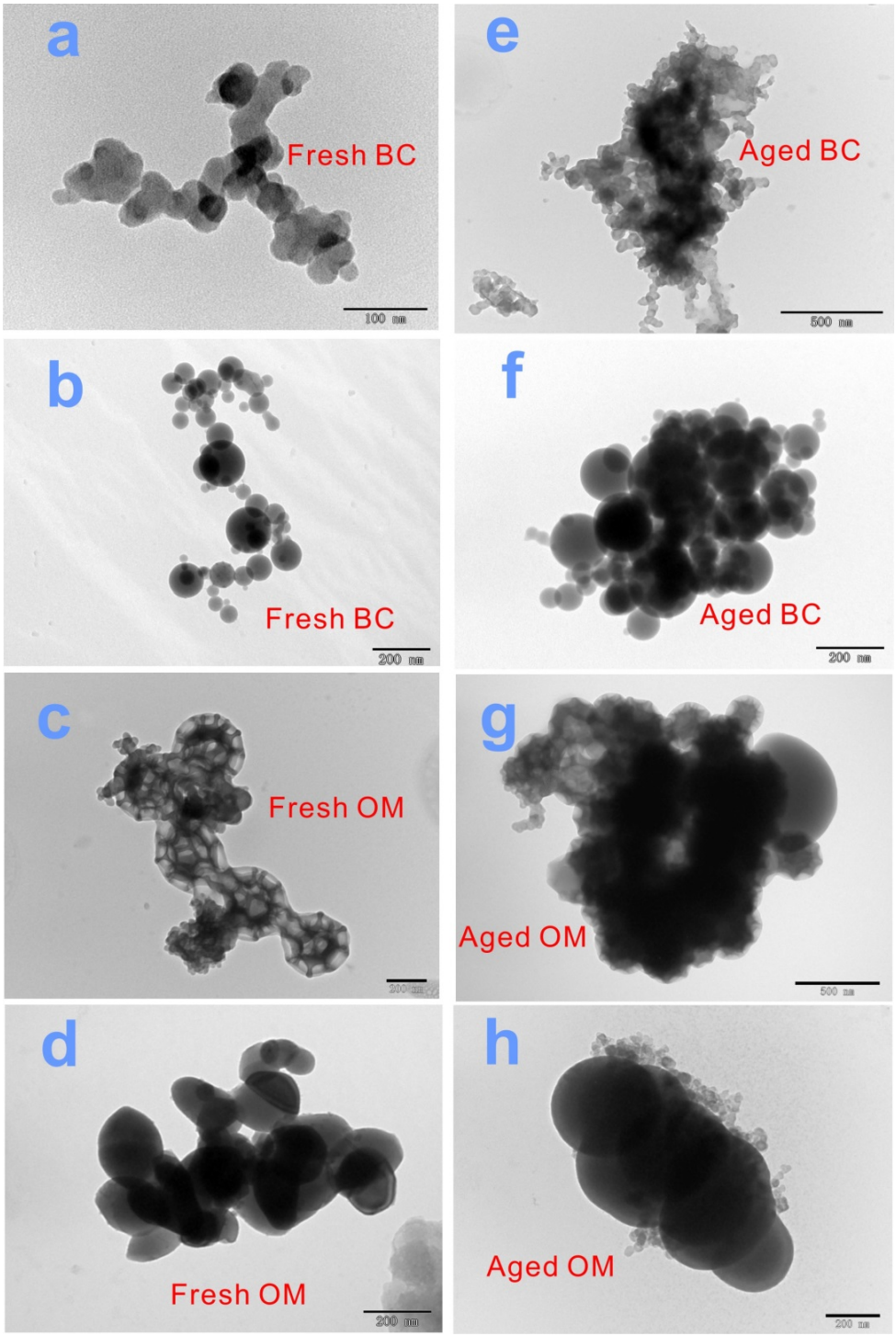

612

613

614

615 **Figure 5**

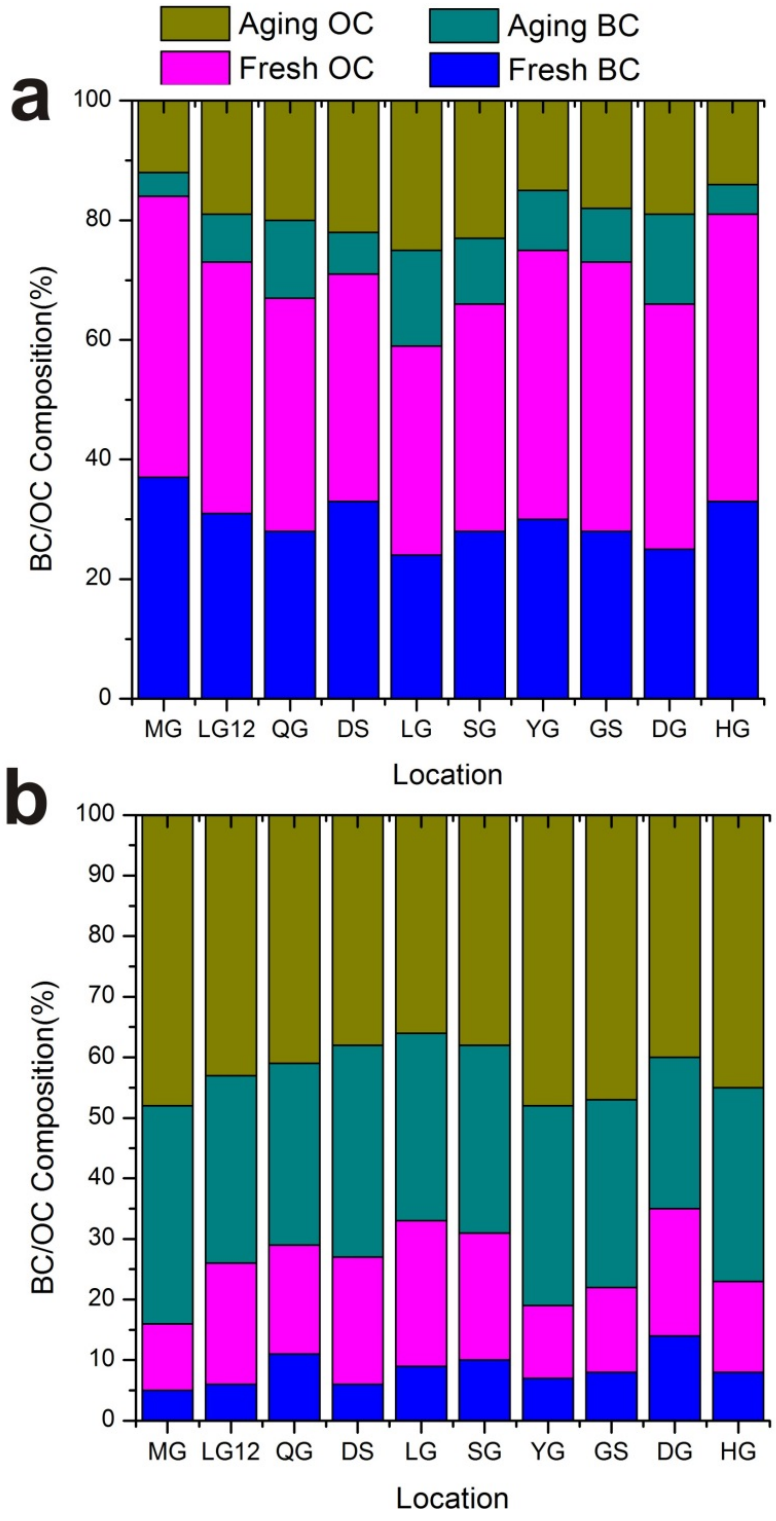

616

617

618

619 **Figure 6**

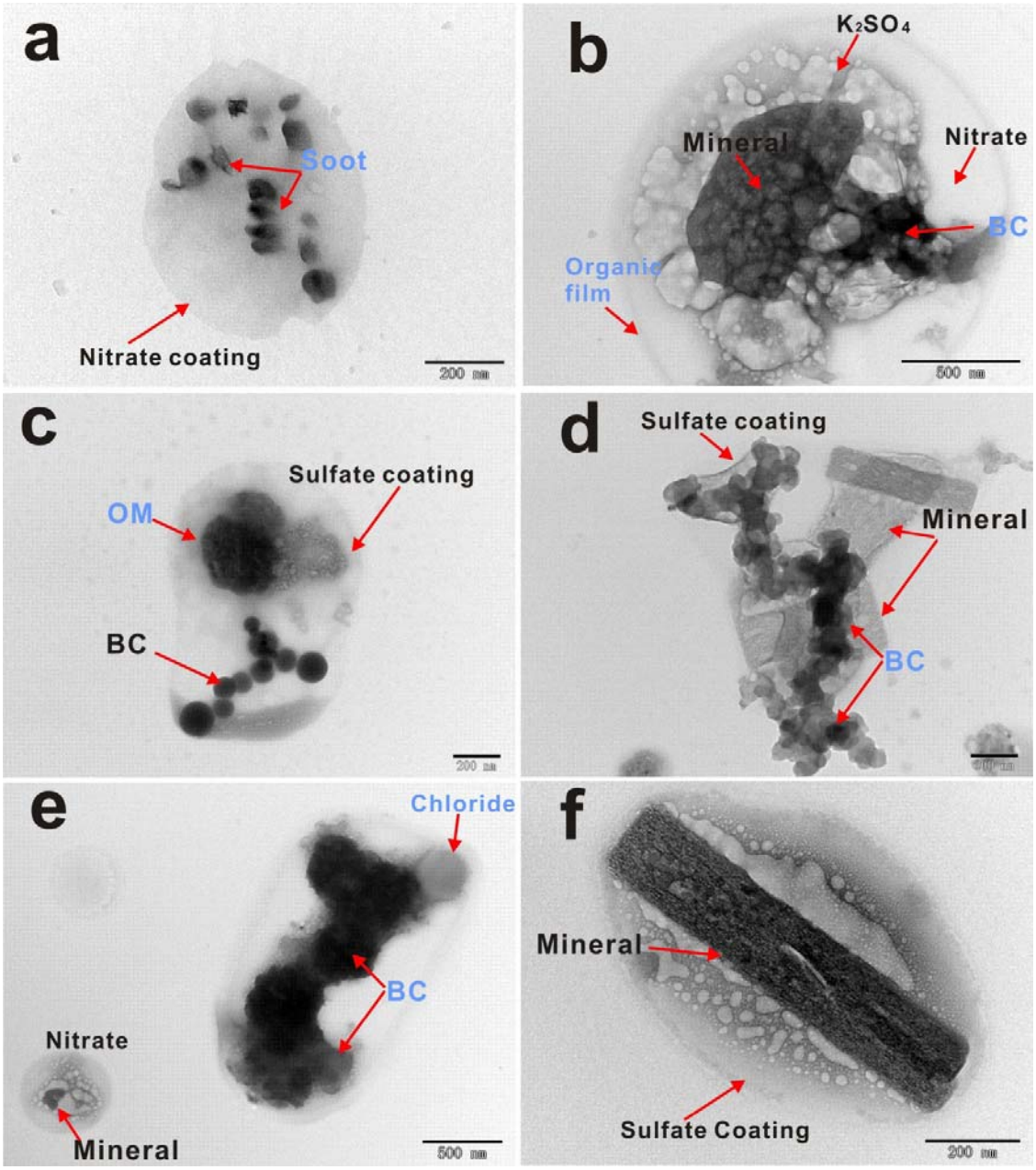

620

621

622

Figure 7

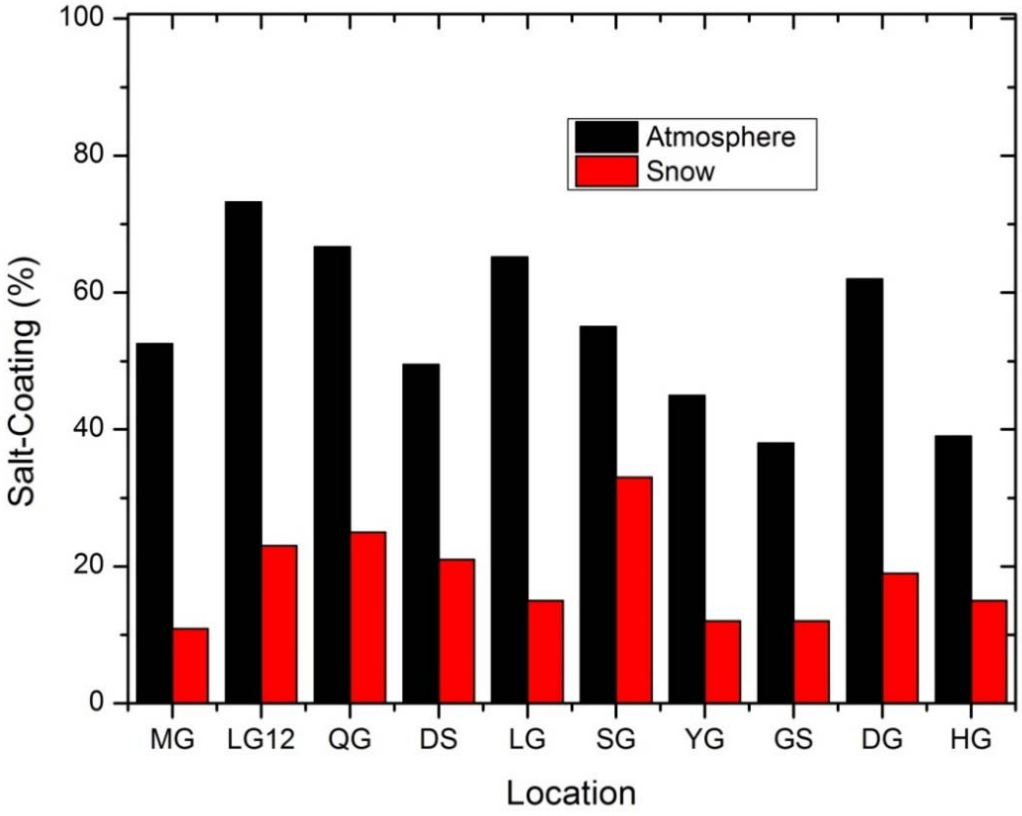
100
80
60
40
20
0
Salt-Coating (%)
Atmosphere
Snow
MG
LG12
QG
DS
LG
SG
YG
GS
DG
HG
Location

637

638

639 **Figure 8**

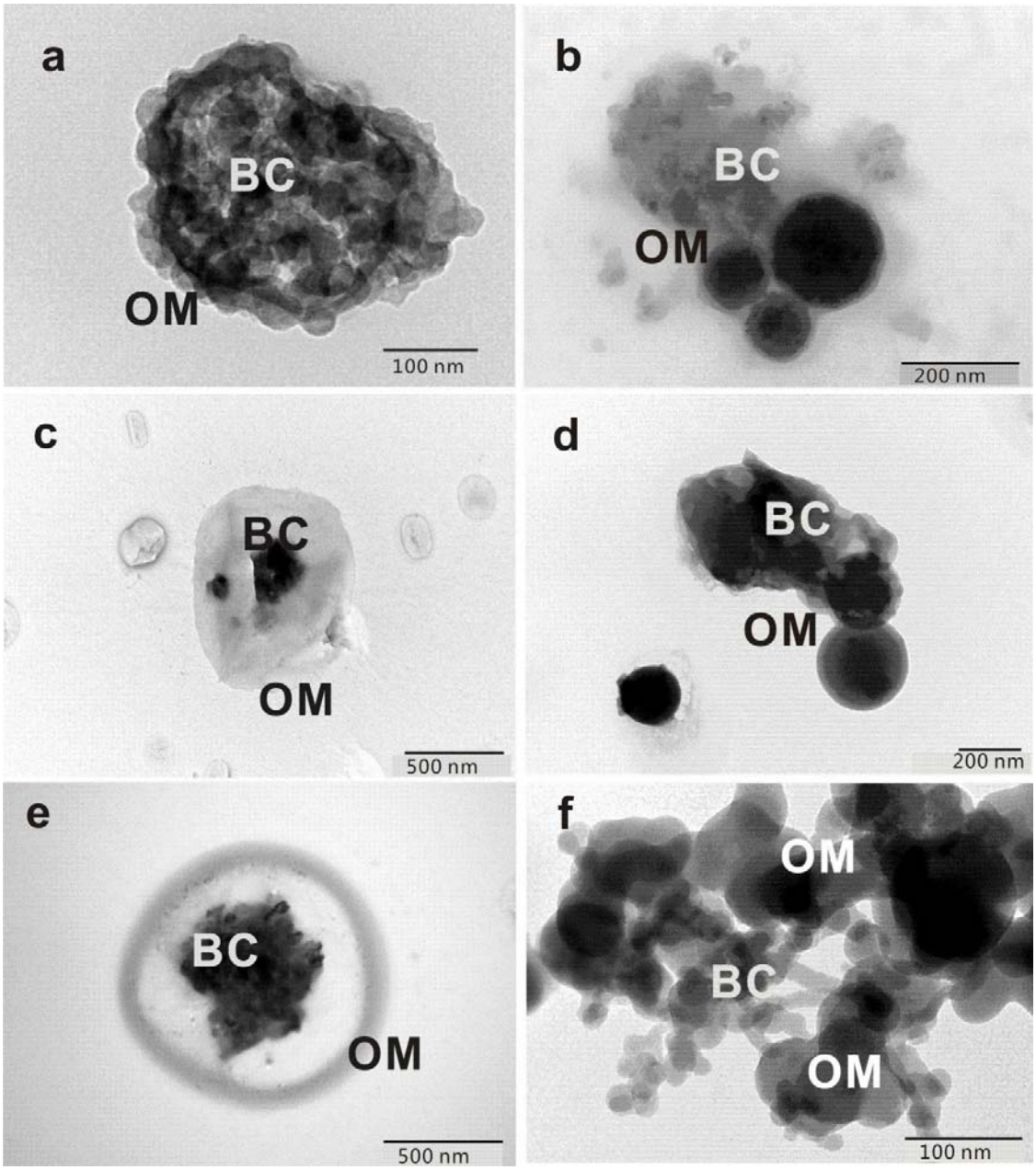

640

641

642

643

644 **Figure 9**

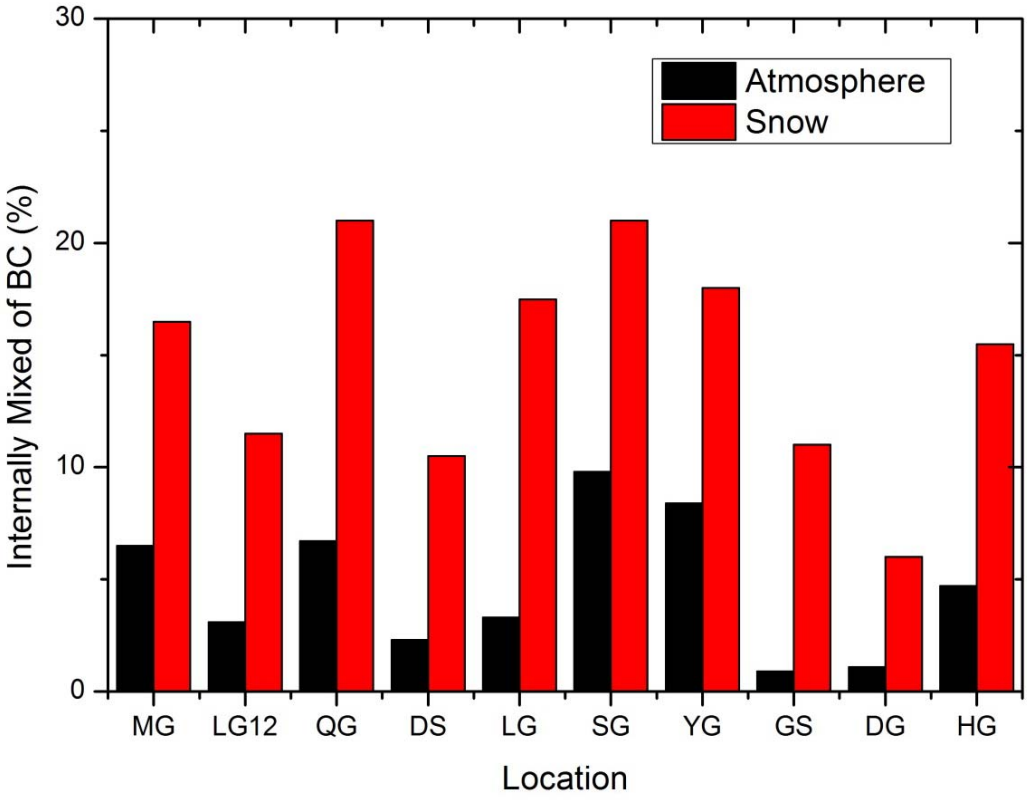

645

646

647

648

649

650

651

652

653

654 **Figure 10**

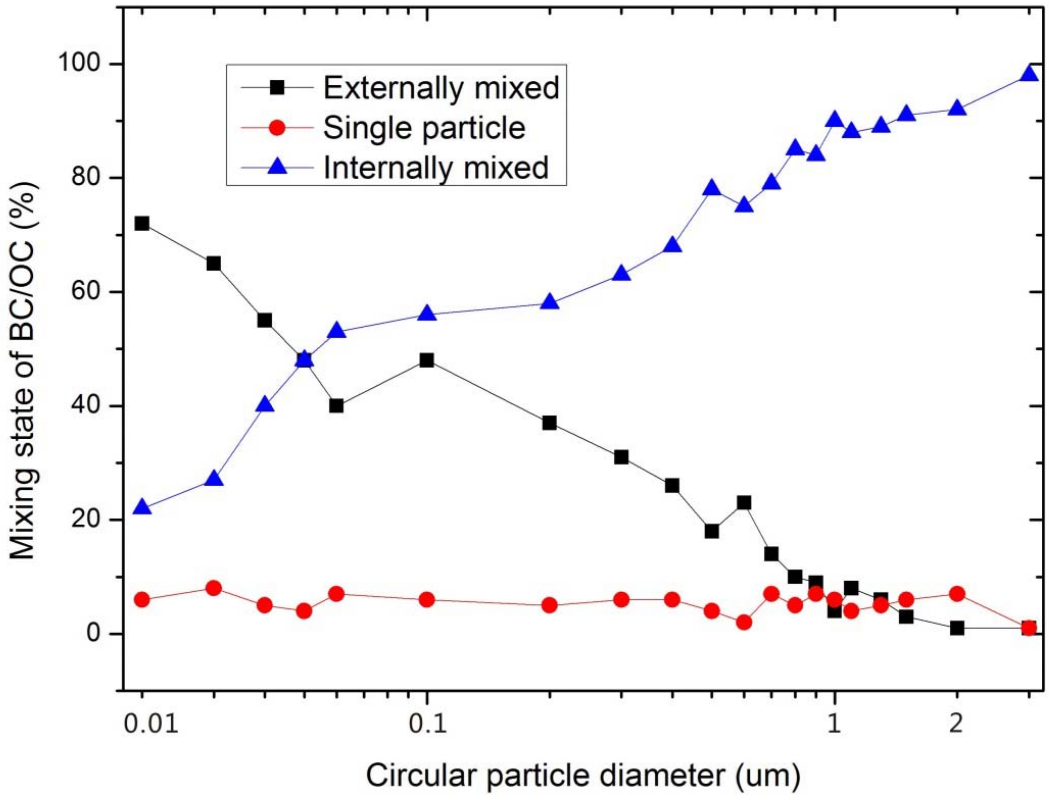

655

656

657

658

659

660

661

662

663

Figure 11

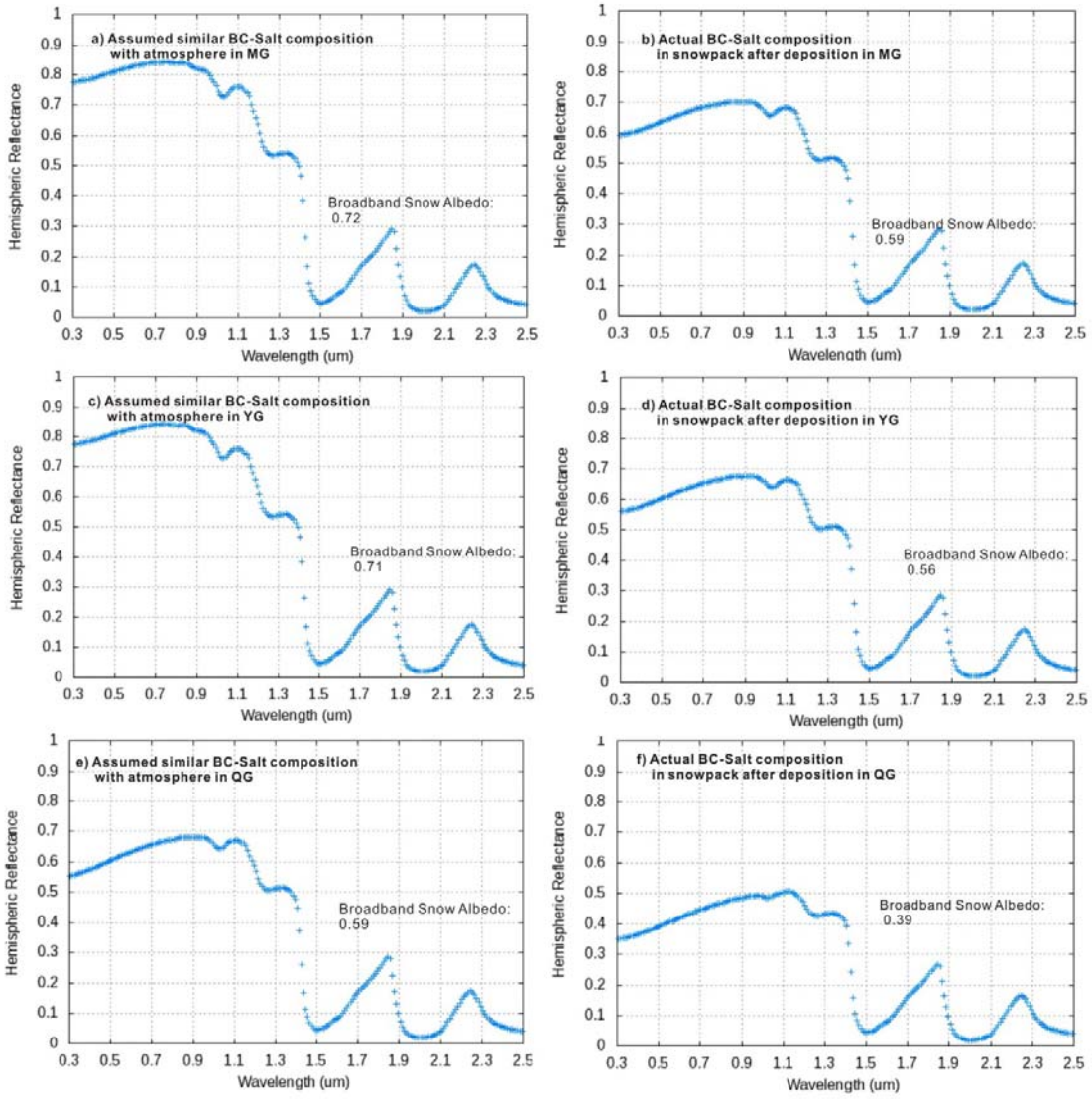
a) Assumed similar BC-Salt composition with atmosphere in MG
Broadband Snow Albedo: 0.72
b) Actual BC-Salt composition in snowpack after deposition in MG
Broadband Snow Albedo: 0.59
c) Assumed similar BC-Salt composition with atmosphere in YG
Broadband Snow Albedo: 0.71
d) Actual BC-Salt composition in snowpack after deposition in YG
Broadband Snow Albedo: 0.56
e) Assumed similar BC-Salt composition with atmosphere in QG
Broadband Snow Albedo: 0.59
f) Actual BC-Salt composition in snowpack after deposition in QG
Broadband Snow Albedo: 0.39
Hemispheric Reflectance
Wavelength (um)

673

674

675

676 **Figure 12**

677

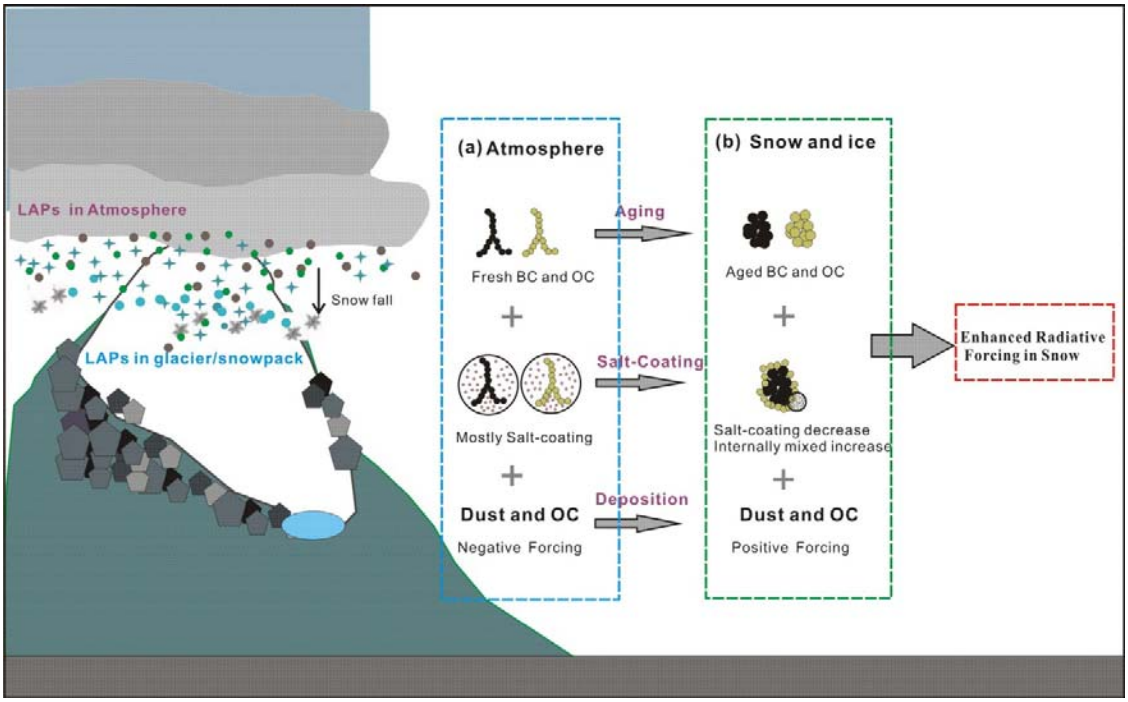

678

679